Submitted to the
32nd International Conference on High Energy Physics
August 16 - 22, 2004, Beijing, China

Abstract: 5-0294 **Session: QCDhard**

Multijet production in deep inelastic scattering at HERA

ZEUS Collaboration

26. July 2004

Abstract

Multijet production rates in neutral current deep inelastic scattering have been measured in the range of boson virtualities $10 < Q^2 < 5000\,\text{GeV}^2$. The data were taken at the ep collider HERA with centre-of-mass energy $\sqrt{s} = 318\,\text{GeV}$ using the ZEUS detector and correspond to an integrated luminosity of $82.2\,\text{pb}^{-1}$. Jets were identified in the Breit frame using the k_T cluster algorithm in the longitudinally invariant inclusive mode . Measurements of differential multijet cross sections are presented as functions of jet transverse energy ($E^{\text{jet}}_{T,B}$), pseudorapidity ($\eta^{\text{jet}}_{\text{LAB}}$) and Q^2 with $E^{\text{jet}}_{T,B} > 5\,\text{GeV}$ and $-1 < \eta^{\text{jet}}_{\text{LAB}} < 2.5$. Next-to-leading-order QCD calculations describe the data well. The value of the strong coupling constant $\alpha_s(M_Z)$, determined from the ratio of the inclusive trijet and dijet cross sections, is $\alpha_s(M_Z) = 0.1179 \pm 0.0013\ (\text{stat.})^{+0.0028}_{-0.0046}\ (\text{exp.})^{+0.0061}_{-0.0040}\ (\text{th.})$.

1 Introduction

Measurements of multijet production from initial state hadrons and leptons have been carried out previously in collisions at the SPS [1], the ISR [2], the TEVATRON [3] and at LEP [4] as well as in photoproduction [5] and deep inelastic scattering (DIS) [6] at HERA. Multijet production in DIS at HERA has been used to test the predictions of perturbative QCD (pQCD) calculations over a large range of four-momentum transfer squared Q^2 [7, 8]. Recently the ZEUS and H1 collaborations have determined the strong coupling constant α_s from a variety of measurements of jet production and jet properties in both deep inelastic scattering and photoproduction [7, 9–13].

At leading order (LO) in the strong coupling constant, α_s, dijet production in neutral current DIS proceeds via the boson-gluon-fusion (BGF, $V^*g \rightarrow q\bar{q}$ with $V = \gamma$, Z^0) and QCD-Compton (QCDC, $V^*q \rightarrow qg$) processes. Events with three jets can be seen as dijet processes with an additional gluon radiation or splitting of a gluon into a quark-antiquark pair, and are directly sensitive to $\mathcal{O}(\alpha_s^2)$ QCD effects. The higher sensitivity to α_s and the large number of degrees of freedom of the trijet final state allow the testing of QCD predictions in great detail.

Trijet production in DIS was presented in a H1 publication [14]. In the present analysis, the differential cross sections for the trijet production have been measured with a higher statistical precision. Measurements of the inclusive trijet cross section as a function of Q^2 and the jet transverse energy, $E_{T,B}^{\mathrm{jet}}$, in the Breit frame and the jet pseudorapidity, $\eta_{\mathrm{LAB}}^{\mathrm{jet}}$, in the laboratory frame are presented. Predictions of pQCD calculations at next-to-leading order (NLO) are compared to the measurements. In addition, the analysis includes the first α_s measurement using the cross-section ratio of inclusive trijet to dijet production, $R_{3/2}$, at HERA. In this ratio many experimental and theoretical uncertainties are reduced, thus allowing for an extension of the range of the measurement to low Q^2. The dependence of this ratio on Q^2 was used to determine the strong coupling constant α_s.

2 Experimental set-up

The data used in this analysis were collected during the 1998-2000 running period, when HERA operated with protons of energy $E_p = 920$ GeV and electrons or positrons[1] of energy $E_e = 27.5$ GeV, and correspond to an integrated luminosity of 82.2 ± 1.9 pb^{-1}. A

[1] Here and in the following, the term "electron" denotes generically both the electron (e^-) and the positron (e^+).

detailed description of the ZEUS detector can be found elsewhere [15,16]. A brief outline of the components that are most relevant for this analysis is given below.

Charged particles are measured in the central tracking detector (CTD) [17], which operates in a magnetic field of 1.43 T provided by a narrow superconducting solenoid. The CTD consists of 72 cylindrical drift chamber layers, organized in nine superlayers covering the polar-angle [2] region $15^\circ < \theta < 164^\circ$. The transverse momentum resolution for full-length tracks can be parameterised as $\sigma(p_T)/p_T = 0.0058 p_T \oplus 0.0065 \oplus 0.0014/p_T$, with p_T in GeV. The tracking system was used to measure the interaction vertex with a typical resolution along (transverse to) the beam direction of 0.4 (0.1) cm and also to cross-check the energy scale of the calorimeter.

The high-resolution uranium-scintillator calorimeter (CAL) [18] covers 99.7% of the total solid angle and consists of three parts: the forward (FCAL), the barrel (BCAL) and the rear (RCAL) calorimeters. Each part is subdivided transversely into towers and longitudinally into one electromagnetic section (EMC) and either one (in RCAL) or two (in BCAL and FCAL) hadronic sections (HAC). The smallest subdivision of the calorimeter is called a cell. Under test-beam conditions, the CAL single-particle relative energy resolutions were $\sigma(E)/E = 0.18/\sqrt{E\,(\mathrm{GeV})}$ for electrons and $\sigma(E)/E = 0.35/\sqrt{E\,(\mathrm{GeV})}$ for hadrons.

The luminosity was measured from the rate of the bremsstrahlung process $e^+p \rightarrow e^+\gamma p$. The resulting small angle energetic photons were measured by the luminosity monitor [19], a lead-scintillator calorimeter placed in the HERA tunnel at $Z = -107$ m.

3 Kinematics and event selection

A three-level trigger system was used to select events online [16,20–22]. Neutral current DIS events were selected by requiring that the scattered electron with energy more than 4 GeV was measured in the CAL [23].

The offline kinematic variables Q^2 (four-momentum transfer squared), x_{Bj} (Bjorken scaling variable) and $y = Q^2/(s x_{Bj})$ (s is centre-of-mass energy) were reconstructed by the electron method (e) [24], double angle (DA) method [25] and Jacquet-Blondel (JB) method [26]. The angle of the hadronic system, γ_{had}, corresponds, in the quark-parton

[2] The ZEUS coordinate system is a right-handed Cartesian system, with the Z axis pointing in the proton beam direction, referred to as the "forward direction", and the X axis pointing left towards the centre of HERA. The coordinate origin is at the nominal interaction point. The pseudorapidity is defined as $\eta = -\ln\left(\tan\frac{\theta}{2}\right)$, where the polar angle, θ, is measured with respect to the proton beam direction.

model, to the direction of the scattered quark and was reconstructed from the CAL measurements of the hadronic final state [9].

If γ_{had} was less than 90° and the scattered electron track could be well reconstructed by the CTD, the DA method was used; otherwise, the electron method was used. The offline selection of DIS events was similar to the one used in a previous measurement [27] and based on the following requirements:

- E'_e>10 GeV, where E'_e is the scattered electron energy, after correction for energy loss in inactive material in front of the CAL, to achieve a high-purity sample of DIS events;
- y_e<0.6, where y_e is y reconstructed by the electron method, to reduce the photoproduction background and improve electron finding efficiency for low energy electrons;
- y_{JB}>0.04, where y_{JB} is y reconstructed by the JB method, to give sufficient accuracy for DA reconstruction of Q^2;
- $\cos\gamma_{had}$<0.7, to ensure good reconstruction of jets in the Breit frame;
- $40<\sum_i(E-P_Z)_i<60$ GeV, where the sum runs over all CAL energy deposits. The lower cut removed background from photoproduction and events with large initial-state QED radiation. The higher cut removed cosmic ray background;
- $\mid Z_{vertex} \mid$ <50 cm, where Z_{vertex} is the reconstructed primary vertex Z-position;
- $\mid X \mid$ >13 or $\mid Y \mid$ >7 cm, where X and Y are the impact positions of the scattered electron on the CAL, to avoid the low acceptance region adjacent to the rear beampipe.

The kinematic range of the analysis is defined as:

$$10 < Q^2 < 5000\,\mathrm{GeV}^2 \text{ and } 0.04 < y < 0.6$$

Jets were reconstructed using the k_T cluster algorithm [28] in the longitudinally invariant inclusive mode. The jet search was conducted in the Breit frame [29]. For each event, the jet search was performed using a combination of track and CAL information, excluding the cells (tracks) associated with the scattered electron. The selected tracks and CAL clusters were treated as massless Energy Flow Objects (EFOs) [30]. The clustering of objects was done according to the Snowmass convention [31].

The jet phase-space is defined by selection cuts on the jet pseudorapidity $\eta^{\rm jet}_{\rm LAB}$ in the laboratory frame and on the jet transverse energy $E^{\rm jet}_{T,B}$ in the Breit frame:

$$-1<\eta^{\rm jet}_{\rm LAB}<2.5 \text{ and } E^{\rm jet}_{T,B}>5\,\mathrm{GeV}$$

Events with two or more jets were selected by requiring the invariant mass of the two highest $E^{\rm jet}_{T,B}$ jets to be:

$$M_{\rm JJ}>25\,\mathrm{GeV}$$

Events with three or more jets were selected by requiring the invariant mass of the three highest $E_{T,B}^{\rm jet}$ jets to be:

$$M_{3\rm J} > 25\,{\rm GeV}$$

These requirements were necessary to ensure a reliable prediction of the cross sections to next-to-leading order, see Section 5.

After all cuts, 37089 events with two or more jets, including 13665 events with three or more jets, remained.

4 Monte Carlo simulation

Monte Carlo (MC) simulations were used to correct the data for detector and resolution effects, for inefficiencies of the event selection and jet reconstruction, as well as for QED effects. Neutral current DIS events were generated using the ARIADNE 4.08 program [32] and the LEPTO 6.5 program [33] interfaced to HERACLES 4.5.2 [34] via DJANGO 6.2.4 [35]. The HERACLES program includes corrections for initial- and final-state radiation, vertex and propagator terms, and two-boson exchange. In case of ARIADNE, the QCD cascade is simulated using the colour-dipole model [36], whereas for LEPTO, the Matrix Elements plus Parton Shower (MEPS) model is used. Both models use the Lund string model [37] as implemented in JETSET 7.4 [38, 39] for the hadronisation.

The ZEUS detector response was simulated with a program based on GEANT 3.13 [40]. The generated events were passed through the simulated detector, subjected to the same trigger requirements as the data, and processed by the same reconstruction and offline programs.

Global event variables (e.g. Q^2, y) are well described by both the ARIADNE and LEPTO MC models after reweighting (Section 6). The LEPTO simulation gives a better overall description of the $E_{T,B}^{\rm jet}$ and invariant mass distributions. Therefore, the events generated with the LEPTO program were used to determine the acceptance corrections. The events generated with ARIADNE were used to estimate the systematic uncertainty coming from the treatment of the parton shower.

5 NLO QCD calculations

The NLO calculations were carried out in the $\overline{\rm MS}$ scheme for five massless quark flavors with the program NLOJET [41] using either CTEQ6 [42], CTEQ4 [43] or MRST99 [44] for the proton parton density functions (PDFs). NLOJET provides a prediction of the trijet production cross sections to next-to-leading order, i.e. including all terms of $\mathcal{O}(\alpha_s^3)$. It was checked that the LO and NLO calculations from NLOJET agree with those of DISENT [45] at the 1-2% level for the dijet cross sections when a fixed α_{EM} coupling is used, the renormalisation scale μ_R^2 is set to $(\bar{E}_T^2 + Q^2)/4$, and the factorization scale μ_F^2 is set to Q^2. For dijets (trijets) $\bar{E}_T$ is the average E_T of the two (three) highest E_T jets in a given event.

For comparison with the data, the CTEQ6 PDF was used and the renormalisation and factorization scales were both chosen to be $(\bar{E}_T^2 + Q^2)/4$ for best description of the data. The strong coupling constant was set to the CTEQ6 parameterisation value $\alpha_s(M_Z) = 0.1179$ and evolved according to the two-loop solution of the renormalization group equation.

The NLO QCD predictions were corrected for hadronisation effects using a bin-by-bin procedure. Hadronisation correction factors were defined for each bin as the ratio of the parton-level to hadron-level cross section and were calculated using the LEPTO MC program. The correction factors were in the range $1.15 - 1.35$ for most of the phase space.

6 Corrections and systematic uncertainties

The jet transverse energy was corrected for energy losses in the inactive material in front of the CAL using the samples of MC simulated events [46,47]. The cross sections for jets of hadrons in bins of Q^2, $E_{T,B}^{\rm jet}$ and $\eta_{\rm LAB}^{\rm jet}$ were obtained by applying a bin-by-bin correction to the measured jets distributions using the LEPTO program. The corrections take into account the efficiency of the trigger, the selection criteria and the purity and efficiency of the jet reconstruction. An additional MC correction from the LEPTO program was applied to the measured cross sections to account for QED effects. The LEPTO sample was reweighted to improve the level of agreement with the Q^2 distribution of the data [21,22]. After this reweighting, all other kinematic distributions were found to agree with the data. The difference in the LEPTO correction factors before and after reweighting was negligible (<0.4%).

A detailed study of the experimental systematic uncertainties was performed [21,22]. The main sources contributing to the systematic uncertainties are listed below:

- *jet pseudorapidity cut* - a change of ± 0.1 (corresponding to the resolution) in the $\eta_{\rm LAB}^{\rm jet}$ cuts imposed on the jets in the laboratory frame for both data and MC simulated events;
- *jet transverse energy and invariant mass cuts* - $E_{T,B}^{\rm jet}$ and $M_{\rm JJ}(M_{\rm 3J})$ were simultaneously varied by the corresponding resolution near the cuts for both data and MC simulated events. Along with the previous systematic check, this takes into account the differences between the data and the MC simulation;

- *use of different parton shower model* - using ARIADNE instead of LEPTO to evaluate the acceptance corrections;
- *the absolute energy scale of the CAL* - varying $E_{T,B}^{\rm jet}$ by its uncertanity of $\pm 1\%(>10\,{\rm GeV})$ and $\pm 3\%(<10\,{\rm GeV})$ for MC simulated events [9].

The systematic uncertainties not associated with the absolute energy scale of the CAL were added in quadrature to the statistical uncertainties and are shown on the figures as error bars. The uncertainty due to the absolute energy scale of the CAL is shown separately as a shaded band.

The main contributions to the theoretical uncertainties of the NLO QCD predictions are:

- uncertainties in the hadronisation correction, which were estimated by using the ARIADNE program to calculate the hadronisation correction factors instead of the LEPTO program;
- uncertainties due to terms beyond NLO, which were estimated by varying both μ_R and μ_F between $(\bar{E}_T^2 + Q^2)$ and $(\bar{E}_T^2 + Q^2)/16$;
- uncertainties in the proton PDFs, which were estimated by repeating the calculations using 40 additional sets obtained under different theoretical assumptions as part of the CTEQ6 release.

The total theoretical uncertainty was obtained by adding in quadrature the individual uncertainties listed above.

7 Results

7.1 Differential cross sections

The differential trijet cross sections as functions of $E_{T,B}^{\rm jet}$ are presented in Figure 1. The three jets were ordered in $E_{T,B}$ ($E_{T,B}^{\rm jet,1} > E_{T,B}^{\rm jet,2} > E_{T,B}^{\rm jet,3}$). The observed decrease of the cross section for the first jet towards small values of $E_{T,B}$ is caused by the $E_{T,B}$ ordering imposed in addition to the requirement that the second and third jet have $E_{T,B} > 5\,{\rm GeV}$. For the second jet, a similar but less pronounced effect is observed. The NLO predictions using NLOJET, corrected for hadronisation effects, are compared to the data. The QCD predictions provide a good description of both the shape and magnitude of the measured cross sections, even at low $E_{T,B}$.

Figure 2 shows the differential trijet cross sections as functions of $\eta_{\rm LAB}^{\rm jet}$. The three jets were ordered in $\eta_{\rm LAB}^{\rm jet}$ ($\eta_{\rm LAB}^{jet,1} > \eta_{\rm LAB}^{\rm jet,2} > \eta_{\rm LAB}^{\rm jet,3}$). Figure 3 shows both the differential dijet and trijet cross section as functions of Q^2. In Figs. 2-3, the data is well described by the NLO QCD predictions.

7.2 Cross-section ratio and determination of α_s

Figure 4 shows the cross-section ratio $R_{3/2}$ of trijet cross section to dijet cross section, as a function of Q^2. The correlated systematic and the renormalisation scale uncertainties cancel in the ratio. The agreement between the data and NLO predictions is good within the substantially reduced uncertainties (experimental $\sim 5\%$, theoretical $\sim 7\%$) compared with uncertainties in dijet and trijet cross sections.

The measurement of $R_{3/2}$ as a function of Q^2 was used to determine $\alpha_s(M_Z)$ with a method similar to that of a previous publication [7]:

- the NLO QCD calculation of $R_{3/2}$ was performed for five sets of the CTEQ4 "A-series" obtained assuming $\alpha_s(M_Z)$=0.110, 0.113, 0.116, 0.119, 0.122 , respectively [43].
- for each bin, i, in Q^2, the NLO QCD calculations, corrected for hadronisation effects, were used to parameterise the $\alpha_s(M_Z)$ dependence of $R_{3/2}$ according to the functional form:

  $$[R_{3/2}(\alpha_s(M_Z))]^i = C_1^i \cdot \alpha_s(M_Z) + C_2^i \cdot \alpha_s^2(M_Z).$$

  C_1^i and C_2^i are fitting parameters. This simple parameterisation gives a good description of the $\alpha_s(M_Z)$ dependence of $R_{3/2}(Q^2)$ over the entire α_s range spanned by the PDF sets;
- the value of $\alpha_s(M_Z)$ was then determined by a χ^2-fit of the above function to the measured $R_{3/2}(Q^2)$ values.

This procedure correctly handles the complete α_s-dependence of the NLO differential cross sections (the explicit dependence coming from the partonic cross sections and the implicit one coming from the PDFs) in the fit, while preserving the correlation between α_s and the PDFs. The CTEQ4 PDF was chosed because it provides more sets with different $\alpha_s(M_Z)$ values than the MRST99 PDF. The CTEQ6 PDF doesn't have different $\alpha_s(M_Z)$ sets and therefore was not used.

Taking into account only the statistical errors on the measured cross-section ratio, $\alpha_s(M_Z)$ is found to be $\alpha_s(M_Z) = 0.1179 \pm 0.0013$(stat.). As a cross-check of the extracted value of $\alpha_s(M_Z)$, the fit procedure was repeated by using the three sets of the MRST99 proton PDF: central, $\alpha_s \uparrow\uparrow$ and $\alpha_s \downarrow\downarrow$ [44]. The result is $\alpha_s(M_Z) = 0.1178 \pm 0.0010$(stat.), in very good agreement with the central value determined above. The uncertainty of the extracted value of $\alpha_s(M_Z)$ due to the experimental and theoretical uncertainties were evaluated by repeating the analysis above for each systematic check as described in Section 6. The total experimental systematic uncertainty on the value of $\alpha_s(M_Z)$ is $^{+0.0028}_{-0.0046}$. The largest uncertainty is that due to the energy scale of CAL. The total theoretical uncertainty is $^{+0.0061}_{-0.0040}$ and is dominated by the uncertainties due to the renormalization scale dependence.

The value of $\alpha_s(M_Z)$ as determined from the measurements of $R_{3/2}$ is therefore:

$$\alpha_s(M_Z) = 0.1179 \pm 0.0013 \text{ (stat.)}^{+0.0028}_{-0.0046} \text{ (exp.)}^{+0.0061}_{-0.0040} \text{ (th.)}.$$

The result is in agreement with recent determinations at HERA (Section 1) and in good agreement with the current world average of $\alpha_s(M_Z) = 0.1182 \pm 0.0027$ [48].

8 Summary

The differential dijet and trijet cross sections have been measured in neutral current deep inelastic scattering for $10 < Q^2 < 5000\,\text{GeV}^2$ with high precision. The inclusive trijet cross section has been measured as a function of $E^{\text{jet}}_{T,B}$, $\eta^{\text{jet}}_{\text{LAB}}$ and Q^2. The ratio $R_{3/2}$ of the inclusive trijet and dijet cross section has been measured as function of Q^2. The predictions of perturbative QCD calculations in next-to-leading order give a good description of the dijet and trijet cross sections and the cross-section ratio $R_{3/2}$ over the whole range of Q^2. The value of the strong coupling constant α_s is measured to be $\alpha_s(M_Z) = 0.1179 \pm 0.0013 \text{ (stat.)}^{+0.0028}_{-0.0046} \text{ (exp.)}^{+0.0061}_{-0.0047} \text{ (th.)}$, well in agreement with the current world average of $\alpha_s(M_Z) = 0.1182 \pm 0.0027$.

References

[1] UA1 Coll., G. Arnison et al., Phys. Lett. **B 158**, 494 (1985);
UA2 Coll., J. A. Appel et al., Z. Phys. **C 30**, 341 (1986).

[2] CMOR Coll., A. L. S. Angelis, Nucl. Phys. **B 303**, 569 (1988);
Axial Field Spectrometer Coll., T. Akesson et al., Z. Phys. **C 32**, 317 (1986).

[3] D0 Coll., B. Abbott et al., Phys. Rev. Lett. **86**, 1955 (2001);
D0 Coll., S. Abachi et al., Phys. Rev. **D 53**, 6000 (1996).

[4] P. Lutz, *Proc. Les Arcs 1996, QCD and high energy hadronic interactions*, pp. 223–228. (1996). Prepared for 31st Rencontres de Moriond: QCD and High-Energy Hadronic Interactions, Les Arcs, France, 23-30 Mar 1996;
Z. Nagy and Z. Trocsanyi, Nucl. Phys. Proc. Suppl. **74**, 44 (1999).

[5] ZEUS Coll., J. Breitweg et al., Phys. Lett. **B 443**, 394 (1998).

[6] ZEUS Coll., M. Derrick et al., Phys. Lett. **B 363**, 201 (1995);
H1 Coll., C. Adloff et al., Eur. Phys. J. **C 6**, 575 (1999).

[7] ZEUS Coll., J. Breitweg et al., Phys. Lett. **B 507**, 70 (2001).

[8] H1 Coll., C. Adloff et al., Eur. Phys. J. **C 19**, 429 (2001).

[9] ZEUS Coll., S. Chekanov et al., Phys. Lett. **B 547**, 164 (2002).

[10] ZEUS Coll., S. Chekanov et al., Phys. Lett. **B 558**, 41 (2003).

[11] ZEUS Coll., S. Chekanov et al., Phys. Lett. **B 560**, 7 (2003).

[12] H1 Coll., C. Adloff et al., Eur. Phys. J. **C 21**, 33 (2001).

[13] H1 Coll., C. Adloff et al., Eur. Phys. J. **C 19**, 289 (2001).

[14] H1 Coll., C. Adloff et al., Phys. Lett. **B 515**, 17 (2001).

[15] ZEUS Coll., M. Derrick et al., Phys. Lett. **B 293**, 465 (1992).

[16] ZEUS Coll., U. Holm (ed.), *The ZEUS Detector*. Status Report (unpublished), DESY (1993), available on `http://www-zeus.desy.de/bluebook/bluebook.html`.

[17] N. Harnew et al., Nucl. Inst. Meth. **A 279**, 290 (1989);
B. Foster et al., Nucl. Phys. Proc. Suppl. **B 32**, 181 (1993);
B. Foster et al., Nucl. Inst. Meth. **A 338**, 254 (1994).

[18] M. Derrick et al., Nucl. Inst. Meth. **A 309**, 77 (1991);
A. Andresen et al., Nucl. Inst. Meth. **A 309**, 101 (1991);
A. Caldwell et al., Nucl. Inst. Meth. **A 321**, 356 (1992);
A. Bernstein et al., Nucl. Inst. Meth. **A 336**, 23 (1993).

[19] J. Andruszków et al., Preprint DESY-92-066, DESY, 1992;
ZEUS Coll., M. Derrick et al., Z. Phys. **C 63**, 391 (1994);
J. Andruszków et al., Acta Phys. Pol. **B 32**, 2025 (2001).

[20] ZEUS Coll., J. Breitweg et al., Z. Phys. **C 74**, 207 (1997).

[21] N. Krumnack, *Three Jet Events in Deep Inelastic Scattering*. Ph.D. Thesis, University of Hamburg, 2004.

[22] L. Li, *Multijets in Neutral Current Deep Inelastic Scattering at HERA*. Ph.D. Thesis, University of Wisconsin-Madison, 2004. In preparation.

[23] ZEUS Coll., J. Breitweg et al., Eur. Phys. J. **C 11**, 427 (1999).

[24] K.C. Höger, *Proc. Workshop on Physics at HERA*, W. Buchmüller and G. Ingelman (eds.), Vol. 1, p. 43. Hamburg, Germany, DESY (1992).

[25] S. Bentvelsen, J. Engelen and P. Kooijman, *Proc. Workshop on Physics at HERA*, W. Buchmüller and G. Ingelman (eds.), Vol. 1, p. 23. Hamburg, Germany, DESY (1992).

[26] F. Jacquet and A. Blondel, *Proceedings of the Study for an ep Facility for Europe*, U. Amaldi (ed.), p. 391. Hamburg, Germany (1979). Also in preprint DESY 79/48.

[27] ZEUS Coll., S. Chekanov et al., Eur. Phys. J. **C 23**, 13 (2002);
D. Chapin, *A Measurement of Dijet Production in Neutral Current Deep Inelastic Scattering with ZEUS at HERA*. Ph.D. Thesis, Univeristy of Wisconsin, Madison, 2001. Unpublished.

[28] S.Catani et al., Nucl. Phys. **B406**, 187 (1993).

[29] R.P. Feynman, *Photon-Hadron Interactions*. Benjamin, New York, 1972;
K.H. Streng, T.F. Walsh, P.M. Zerwas, Z. Phys. **C 2**, 237 (1979).

[30] ZEUS Coll., S. Chekanov et al., Preprint hep-ex/0404033, 2004.

[31] J.E. Huth et al., *Research Directions for the Decade. Proceedings of Summer Study on High Energy Physics, 1990*, E.L. Berger (ed.), p. 134. World Scientific (1992). Also in preprint FERMILAB-CONF-90-249-E.

[32] L. Lönnblad, Comp. Phys. Comm. **71**, 15 (1992).

[33] G. Ingelman, A. Edin and J. Rathsman, Comp. Phys. Comm. **101**, 108 (1997).

[34] A. Kwiatkowski, H. Spiesberger and H.-J. Möhring, Comp. Phys. Comm. **69**, 155 (1992). Also in *Proc. Workshop Physics at HERA*, 1991, DESY, Hamburg.

[35] K. Charchula, G.A. Schuler and H. Spiesberger, Comp. Phys. Comm. **81**, 381 (1994).

[36] G. Gusafson and U. Pettersson, Nucl. Phys. **B 306**, 746 (1988).

[37] B. Andersson et al., Phys. Rep. **97**, 31 (1983).

[38] M. Bengtsson and T. Sjöstrand, Comp. Phys. Comm. **46**, 43 (1987).

[39] T. Sjöstrand, Comp. Phys. Comm. **82**, 74 (1994).

[40] R. Brun et al., GEANT3, Technical Report CERN-DD/EE/84-1, CERN, 1987.

[41] Z. Nagy and Z Trocsanyi, Phys. Rev. Lett. **87**, 082001 (2001).

[42] J. Pumplin et al., Preprint hep-ph/0201195, 2002.

[43] H.L. Lai et al., Phys. Rev. **D 55**, 1280 (1997).

[44] A.D. Martin et al., Eur. Phys. J. **C 14**, 133 (2000).

[45] S. Catani and M. H. Seymour, Nucl. Phys. **B 485**, 291 (1997).

[46] ZEUS Coll., M. Derrick et al., Phys. Lett. **B 342**, 417 (1995).

[47] ZEUS Coll., J. Breitweg et al., Eur. Phys. J. **C 8**, 367 (1999).

[48] S. Bethke, Preprint hep-ex/0407021, 2004. Talk given at 7th DESY Workshop on Elementary Particle Theory: Loops and Legs in Quantum Field Theory, Zinnowitz, Germany, 25-30 Apr 2004.

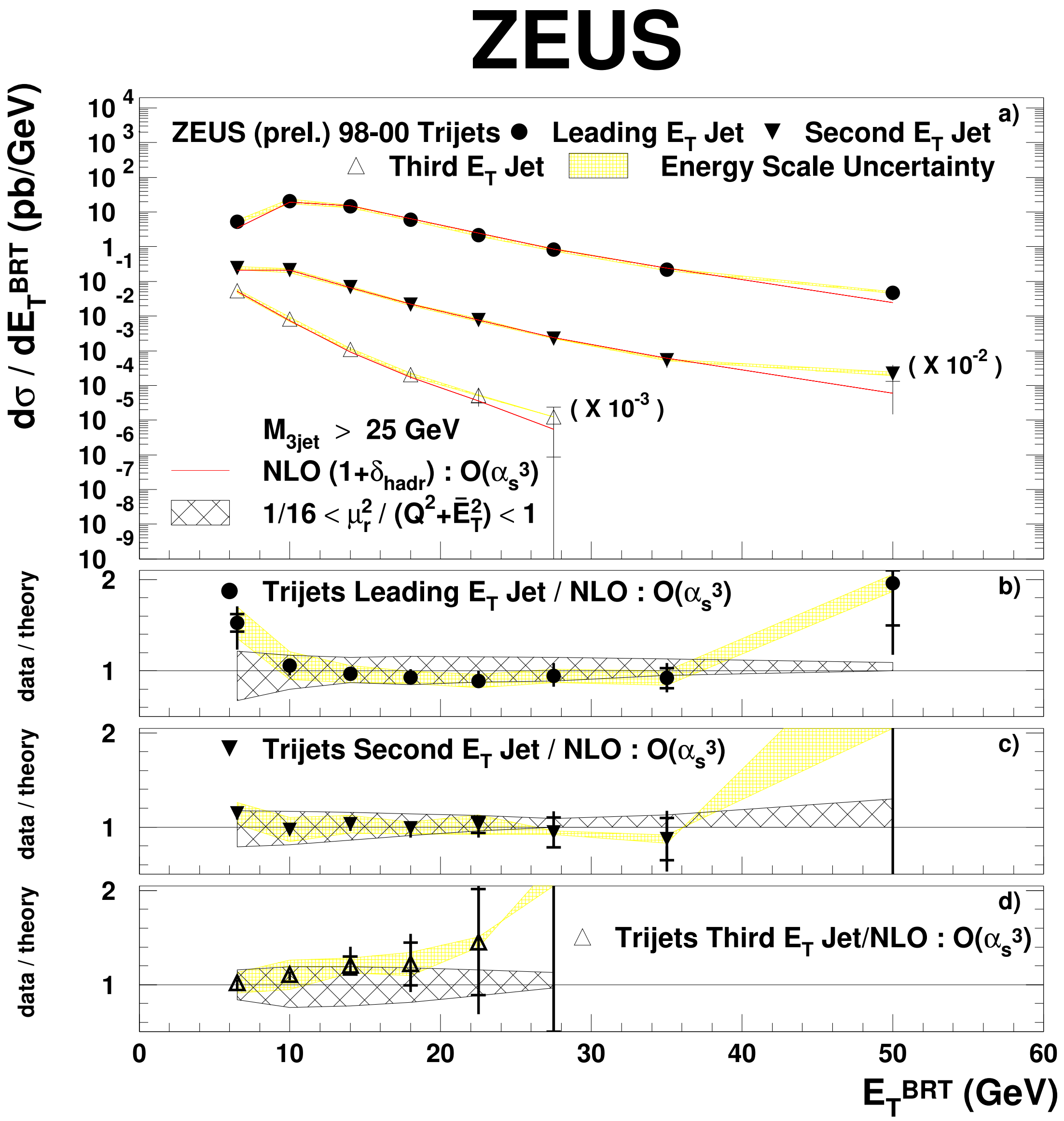

Figure 1: *a) The inclusive trijet cross sections as functions of E_T^{jet} with the jets ordered in E_T. The cross sections of the second and third jet were scaled down for readability only. The inner error bars represent the statistical uncertainties and the outer error bars represent the quadratic sum of all uncertainties. The shaded band indicates the calorimeter energy scale uncertainty. The predictions of perturbative QCD in next-to-leading order is compared to the data. b), c) and d) show the ratio of the data over predictions. The hatched band represents the renormalisation scale uncertainty of the QCD calculation. The NLO was corrected from the parton to hadron level using correction factors obtained from parton and hadron level* LEPTO.

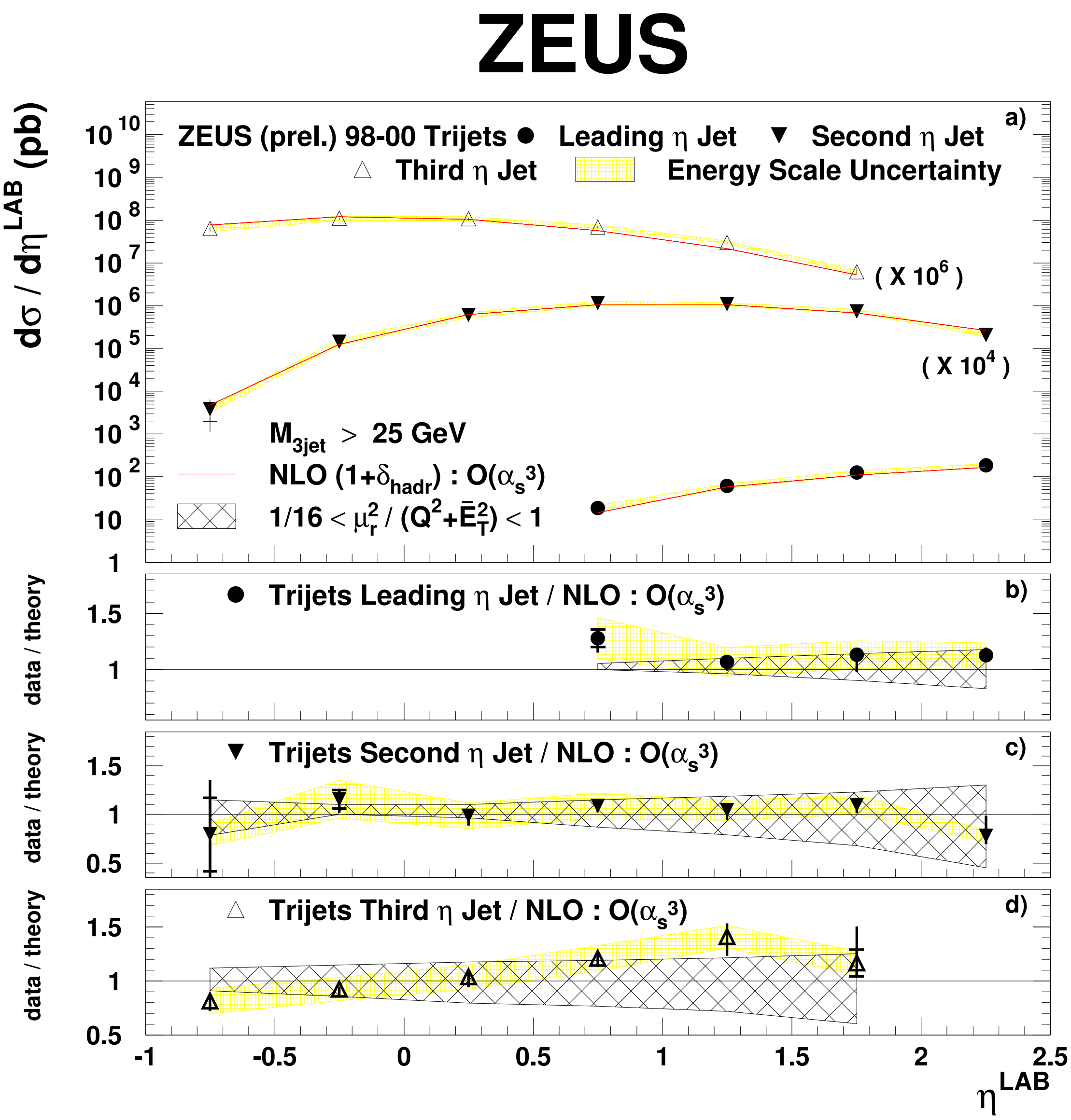

Figure 2: *a) The inclusive trijet cross sections as functions of η^{jet} with the jets ordered in η. The cross sections of the second and third jet were scaled up for readability only. The predictions of perturbative QCD in next-to-leading order is compared to the data. b), c) and d) show the ratio of the data over predictions. Other details are as described in the caption in Fig. 1.*

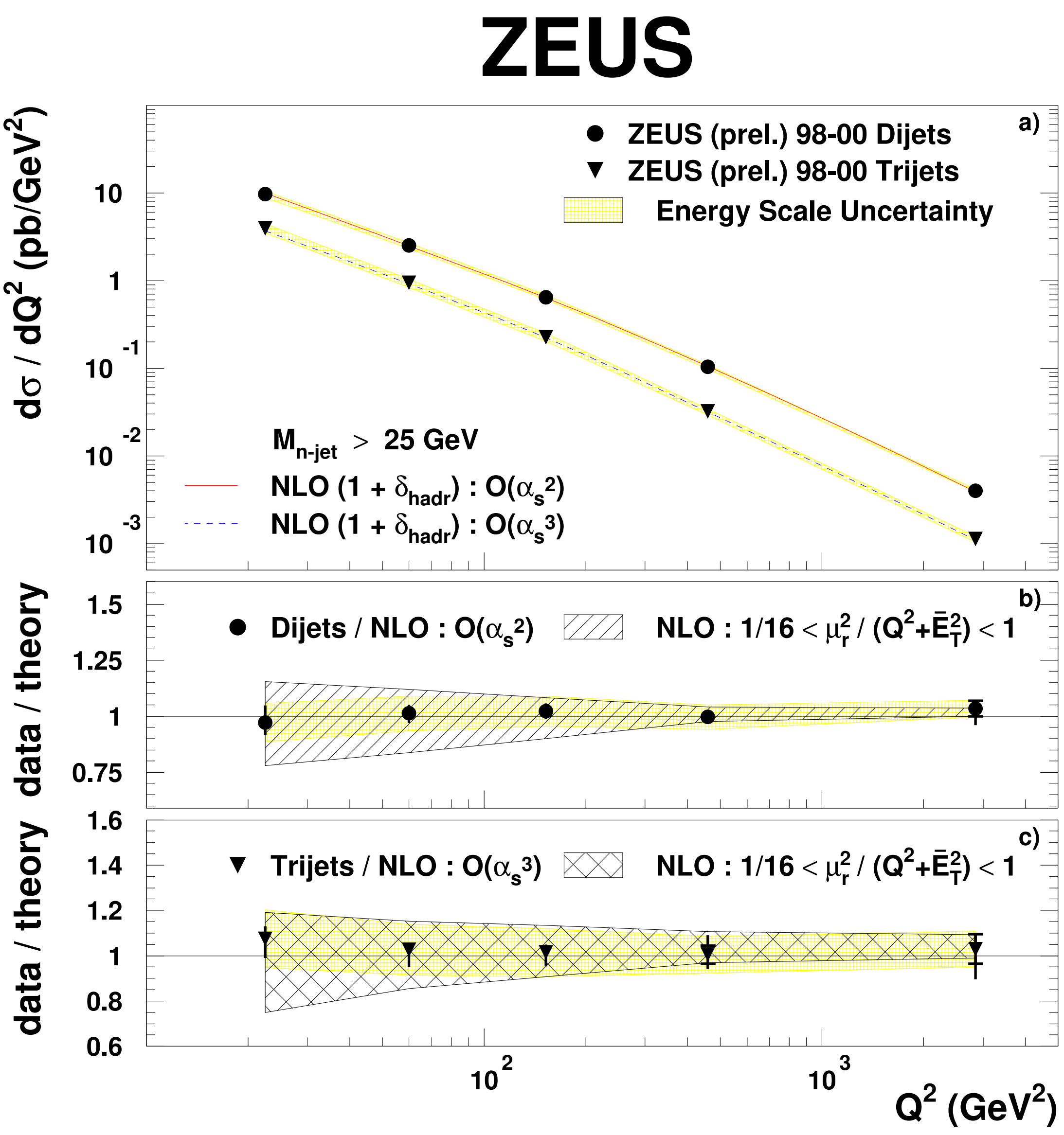

Figure 3: *a) The inclusive dijet and trijet cross sections as functions of Q^2. The predictions of perturbative QCD in next-to-leading order is compared to the data. b) and c) show the ratio of the data over predictions. Other details are as described in the caption in Fig. 1.*

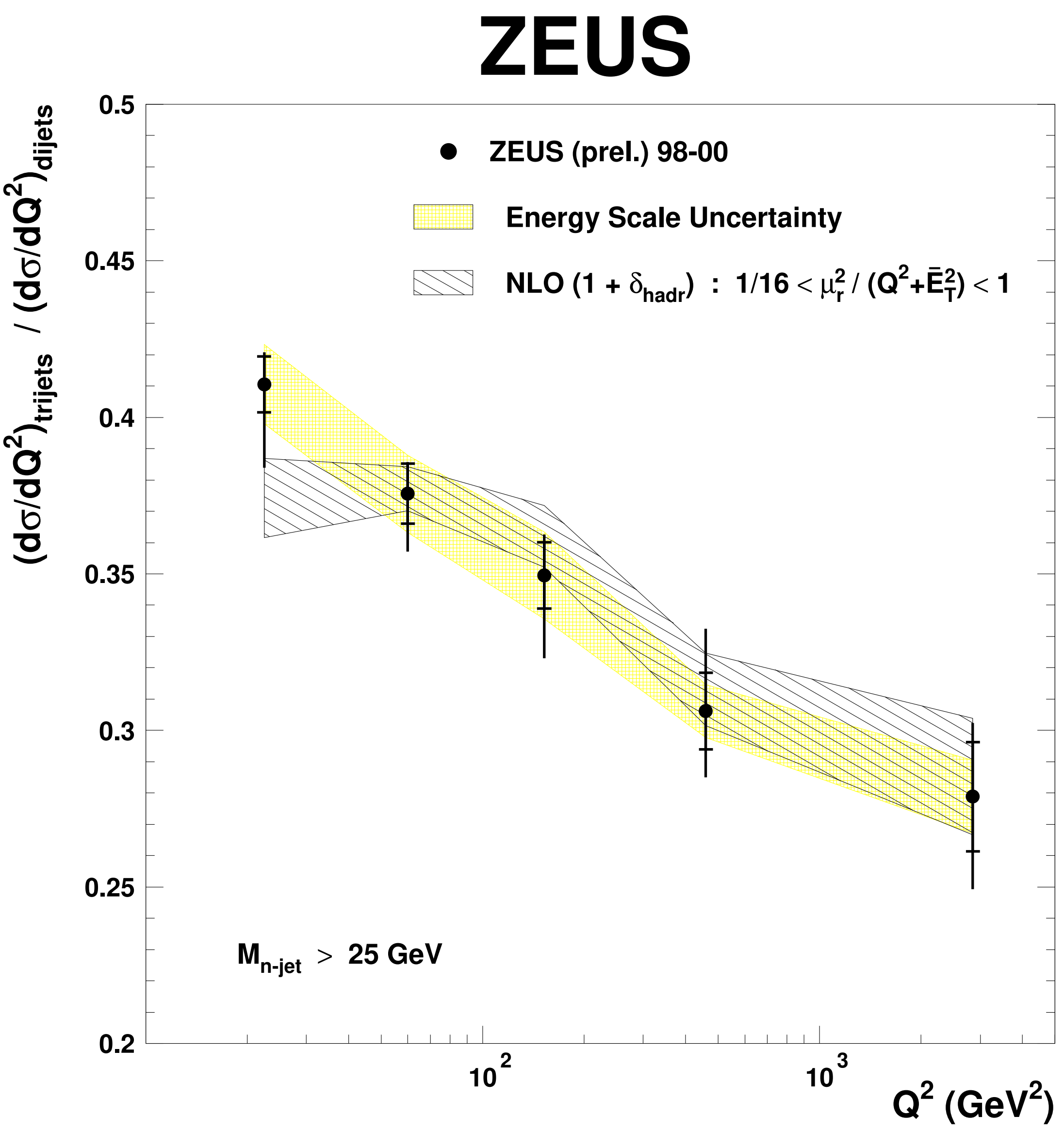

Figure 4: *The ratio of inclusive trijet over dijet cross section as a function of Q^2. The predictions of perturbative QCD in next-to-leading order are compared to the data. Other details are as described in the caption in Fig. 1.*